Electronic Supplementary Material (ESI) for Catalysis Science & Technology.
This journal is © The Royal Society of Chemistry 2024

Electronic Supplementary Information

Experimental section

Materials: All the chemicals used in this study were of analytical grades and were directly utilized without undergoing any purification processes. Nickel nitrate hexahydrate ($Ni(NO_3)_2·6H_2O$), lanthanum nitrate hexahydrate ($La(NO_3)_3·6H_2O$), ruthenium oxide (RuO_2), urea, ammonium fluoride (NH_4F), potassium hydroxide (KOH), sodium chloride (NaCl), sodium carbonate (Na_2CO_3), o-tolidine, potassium permanganate ($KMnO_4$) were procured from Aladdin Industrial Corporation. Acetone, ethanol, and hydrochloric acid (HCl) were obtained from Beijing Chemical Reagent Co., Ltd. (Beijing, China). Natural seawater was gained from Qingdao, Shandong, China. Prior to usage, most of the magnesium and calcium salts present in the natural seawater were eliminated by adding Na_2CO_3. Ni foam (NF) was sourced from Shenzhen Green and Creative Environmental Science and Technology Co., Ltd. The ultrapure water employed for experimental purposes was purified using a Millipore system.

Preparation of La-Ni(OH)$_2$/NF and Ni(OH)$_2$/NF: The La-$Ni(OH)_2$/NF was prepared using a hydrothermal synthesis technique. Initially, a piece of NF (2 × 3 cm^2) underwent sequential ultrasonic cleaning using HCl, ethanol, and deionized water prior to usage. Subsequently, the NF sample was immersed in a solution containing 30 mL deionized water along with 0.86 g $Ni(NO_3)_3·6H_2O$, 0.3 g NH_4F, 0.09 g $La(NO_3)_3·6H_2O$ and 0.9 g urea. The mixture was subjected to ultrasonication for a duration of 30 minutes followed by hydrothermal treatment at a temperature of 120℃ for a period of six hours. Upon reaching room temperature after cooling down, the NF substrate coated with La was retrieved and thoroughly rinsed multiple times using ethanol and water. Preparation of $Ni(OH)_2$/NF was identical to that of La-$Ni(OH)_2$/NF without 0.3 mM $La(NO_3)_3·6H_2O$.

Preparation of RuO_2 and Pt/C on NF: An ink with a uniform consistency (5 mg mL^{-1}) was prepared by adding 5 mg RuO_2 or Pt/C to a solution comprising of 30μL Nafion, 485μL ethanol, and 485μL deionized water using ultrasonication for 0.5 h.

Subsequently, 560 μL catalyst ink was coated onto a treated NF (1 × 1 cm^2) substrate at a loading mass of 2.8 mg cm^{-2}.

Characterization: X-ray diffraction (XRD) data were obtained via X-ray diffraction (Philip D8). Scanning electron microscopy (SEM, ZISS 300) equipped with an energy dispersive X-ray (EDX) facility, transmission electron microscopy (TEM, JEM-F200, JEOL Ltd.), and X-ray photoelectron spectroscopy (XPS, ESCALAB 250 Xi) were applied to research the morphology and compositions of samples. Absorbance data were acquired on ultraviolet-visible (UV-vis) spectrophotometer (Shimadzu UV-2700). ICP-OES was performed on an Inductive Coupled Plasma Emission Spectrometer (iCAD7400).

Electrochemical measurements: The electrochemical measurements were conducted using a CHI660E electrochemical analyzer from CHI instruments, Inc., Shanghai. in a standard three-electrode system. La-$Ni(OH)_2$/NF was used as the working electrode, a graphite rod as the counter electrode, and the Hg/HgO electrode as the reference electrode. The solution temperature was maintained at 25°C throughout all measurements by adjusting air condition and heating support to ensure minimal variation in diffusion coefficient (below 1%). The potentials reported in this study were calibrated to the reversible hydrogen electrode (RHE), unless otherwise specified. This calibration was achieved using the equation: $E_{(RHE)} = E_{(Hg/HgO)} + 0.098 + 0.059 \times pH$. To calculate the Tafel slope, we utilized the Tafel equation: $\eta = b\log j + a$. Where η represents overpotential (V, calculated by $|E - E^*$ HER$|$), j denotes current density (mA cm^{-2}), and b signifies the Tafel slope (mV dec^{-1}). Electrochemical impedance spectroscopy tests were conducted in the frequency range of 10^5 to 0.01 Hz, using a voltage amplitude of 5 mV in a potassium hydroxide solution with a concentration of 1 M. The Cyclic voltammetry (CV) technique was employed to measure the double-layer capacitance (C_{dl}) values for La-$Ni(OH)_2$/NF, $Ni(OH)_2$/NF, RuO_2/NF and NF at various scan rates ranging from 20-180 mV s^{-1} in a potassium hydroxide solution with a concentration of 1 M. The determination of the Faradaic efficiency (FE) for OER was conducted using the drainage technique in a two-compartment H-type cell, with separation achieved by employing a Nafion 117

membrane.The ECSA of the catalyst can be calculated by using the following equation:

$$ECSA = S_{geometric\ area} \times C_{dl}/C_S$$

Where C_{dl} is the experimentally obtained capacitance, C_S is the specific capacitance, and $S_{geometric}$ area is the geometric area of the electrode.

Detection of hypochlorite: The hypochlorite concentration in the electrolyte during long-term seawater electrolysis was measured by o-tolidine method via the redox reaction between hypochlorite and o-tolidine. The testing solution was 0.5 mL o-tolidine in DI water (10 mL). To obtain the calibration curve, different amounts of Cl_2 (2.5, 5, 10, 15, and 25 μL) freshly generated by reacting $KMnO_4$ (500 mg) with HCl (6.0 M, 10 mL) were collected into KOH solution (1.0 M, 0.1 mL) and injected into the testing solution. The UV-vis spectrum was measured to obtain the ClO^- concentration absorbance curve at λ = 436 nm. After long-term seawater electrolysis, a part of the electrolyte (0.1 mL) was added into the testing solution, in which the ClO^- concentration can be determined by comparing the UV-vis spectrum and calibration curve.

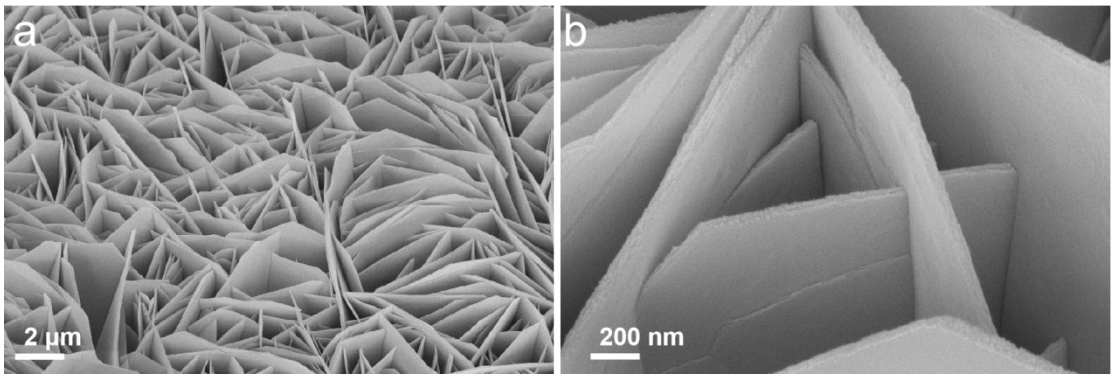

Fig. S1. (a) Low- and (b) high-magnification SEM images of $Ni(OH)_2$/NF.

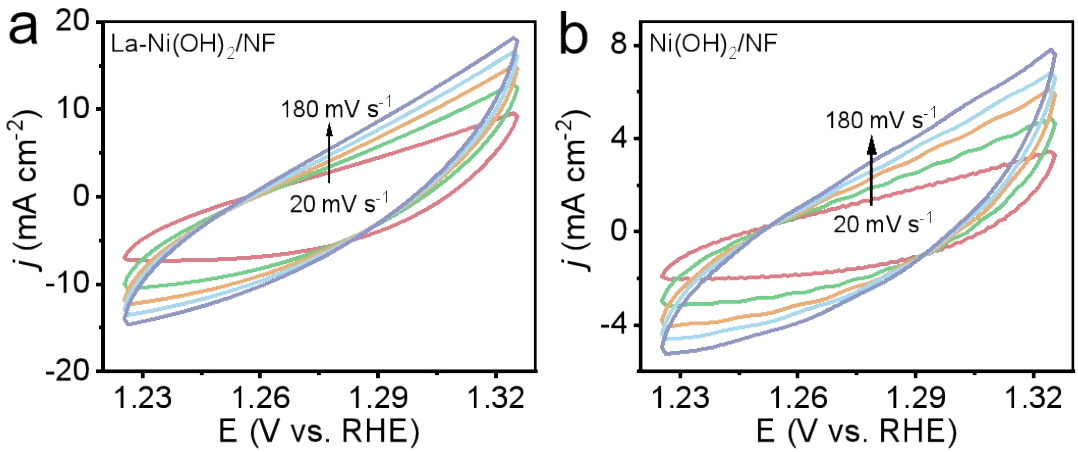

Fig. S2. CV curves of (a) La-Ni(OH)$_2$/NF and (b) Ni(OH)$_2$/NF in 1 M KOH.

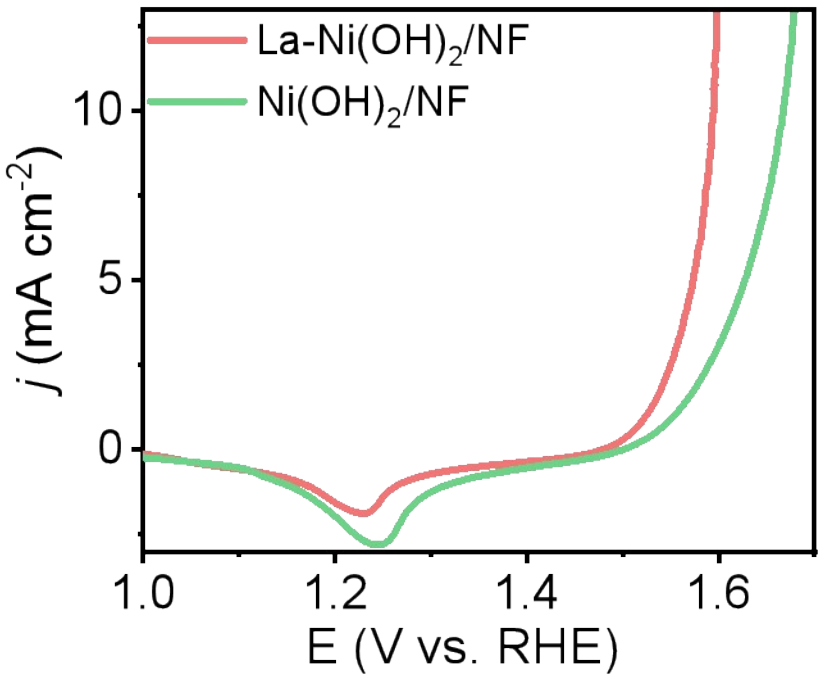

Fig. S3. LSV curves in 1 M KOH for La-$Ni(OH)_2$/NF and $Ni(OH)_2$/NF normalized by the electrochemical active surface area.

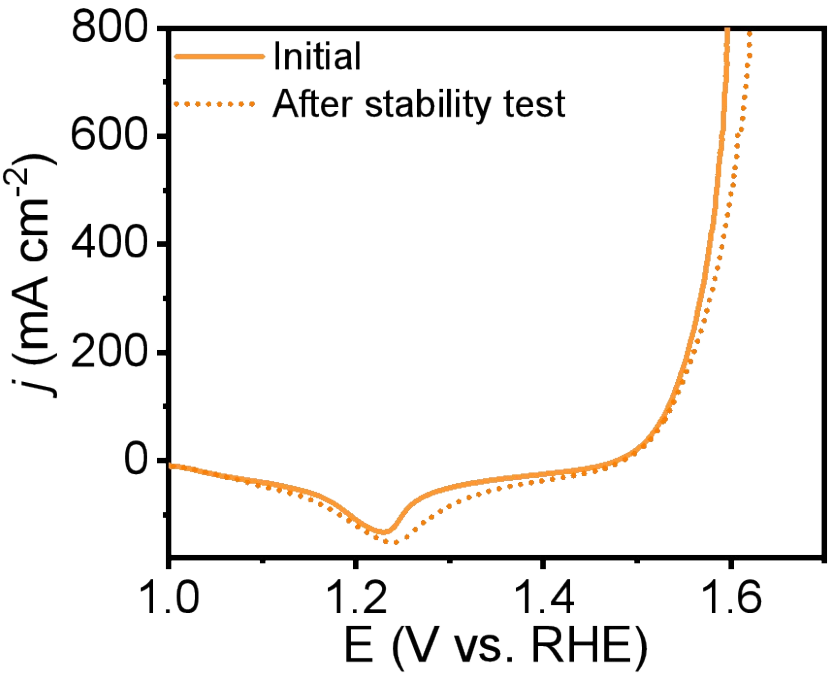

Fig. S4. LSV curves of La-Ni$(OH)_2$/NF before and after the stability test at a current density of 500 mA cm^{-2} in 1 M KOH.

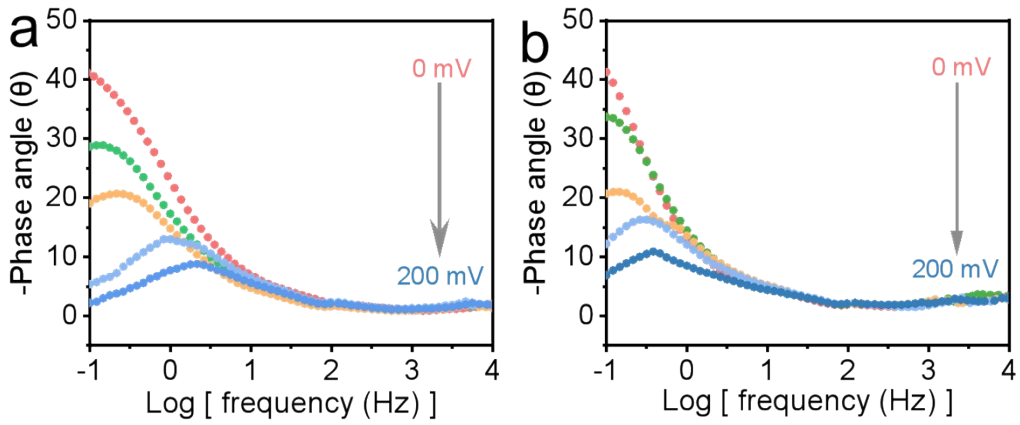

Fig. S5. Bode phase plots of (a) La-Ni(OH)$_2$/NF and (b) Ni(OH)$_2$/NF in 1 M KOH.

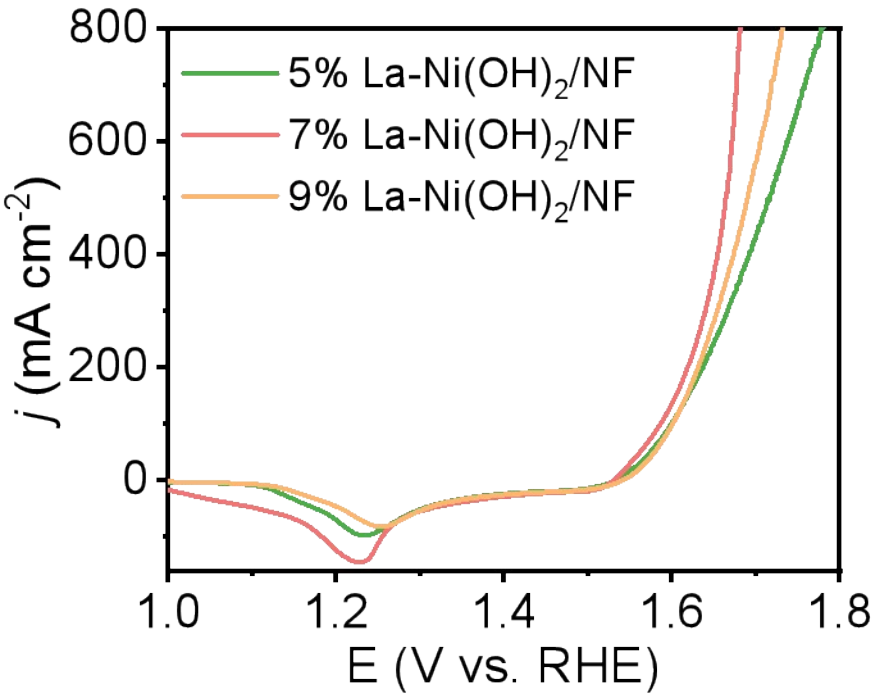

Fig. S6. LSV curves of different contents of La electrocatalysts in 1 M KOH + seawater.

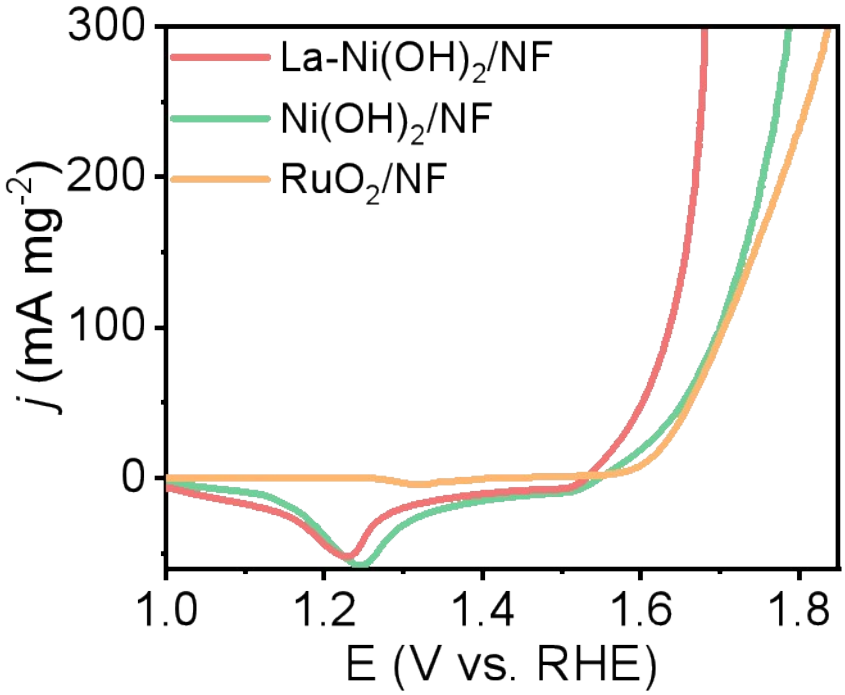

Fig. S7. Mass activity of La-$Ni(OH)_2$/NF, $Ni(OH)_2$/NF and RuO_2/NF in 1 M KOH + seawater.

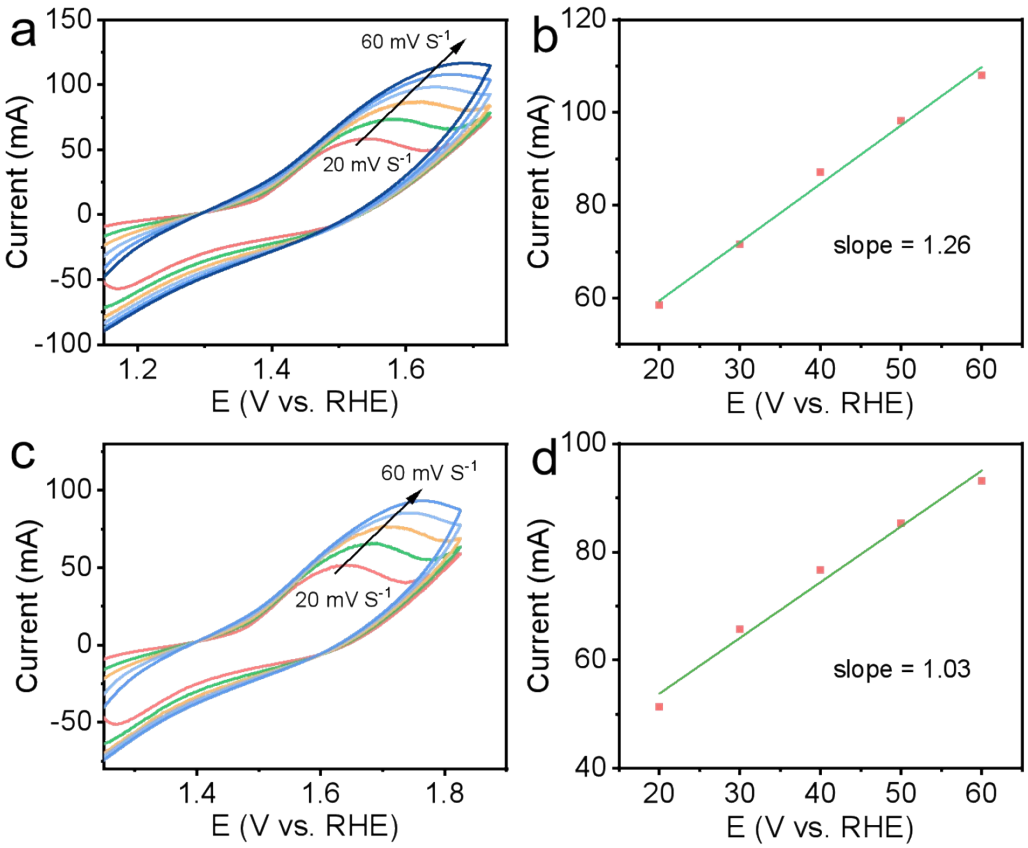

Fig. S8. CV curves for (a) La-$Ni(OH)_2$/NF and (c) $Ni(OH)_2$/NF at different scan rates increasing from 20 to 60 mV s^{-1} in 1 M KOH + seawater. Oxidation peak current versus the scan rate plot for (b) La-$Ni(OH)_2$/NF and (d) $Ni(OH)_2$/NF.

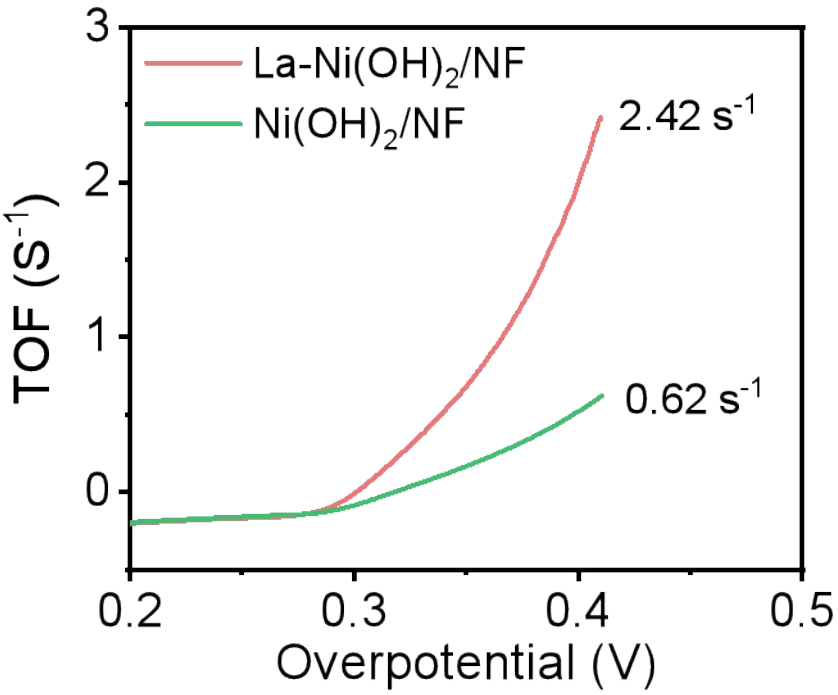

Fig. S9. TOF plots of La-$Ni(OH)_2$/NF and $Ni(OH)_2$/NF.

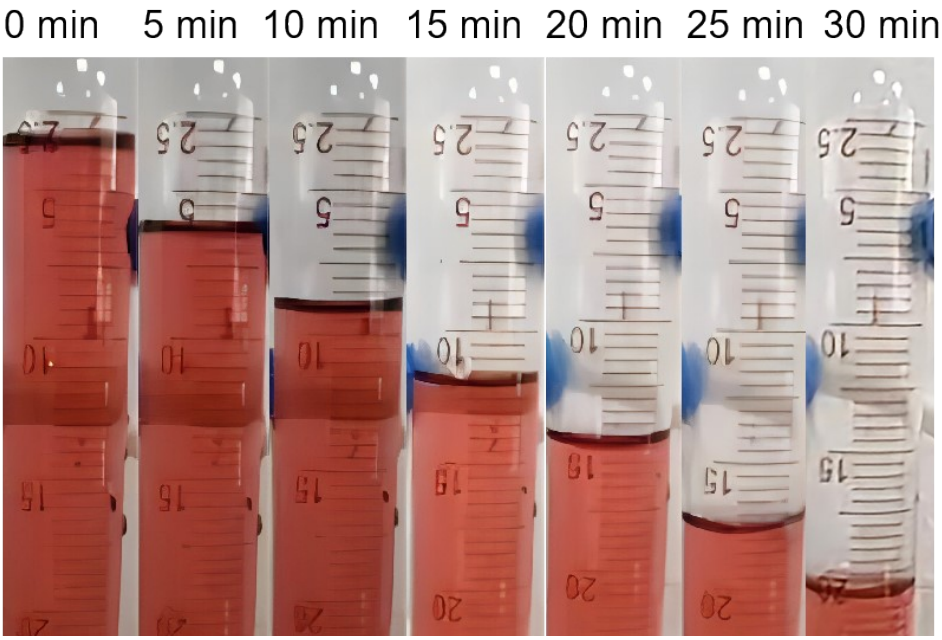

Fig. S10. Collection of oxygen evolved from seawater oxidation at a current density of 500 mA cm^{-2} by drainage method.

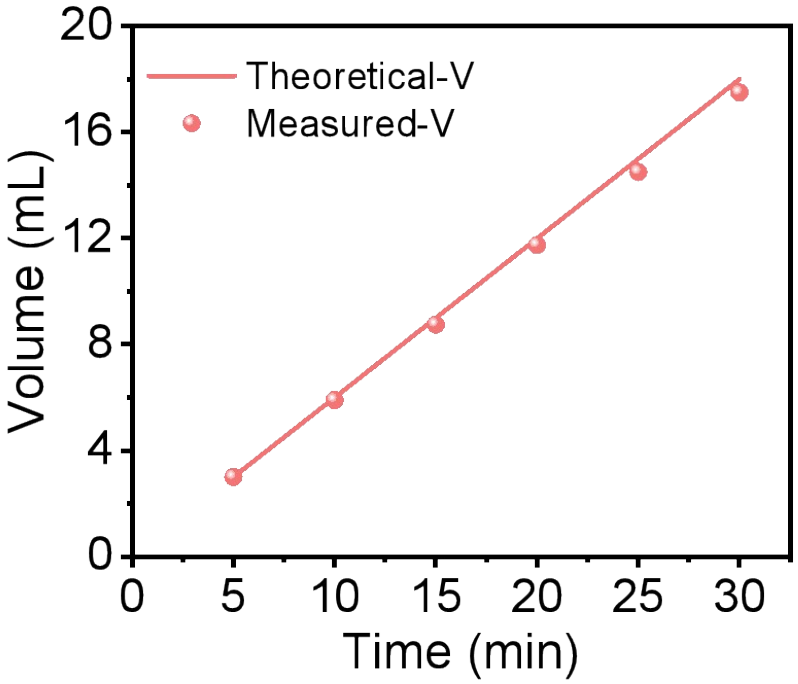

Fig. S11. Comparison between the amount of collected and theoretical O_2 for La-Ni(OH)$_2$/NF at a current density of 500 mA cm^{-2} in 1 M KOH + seawater.

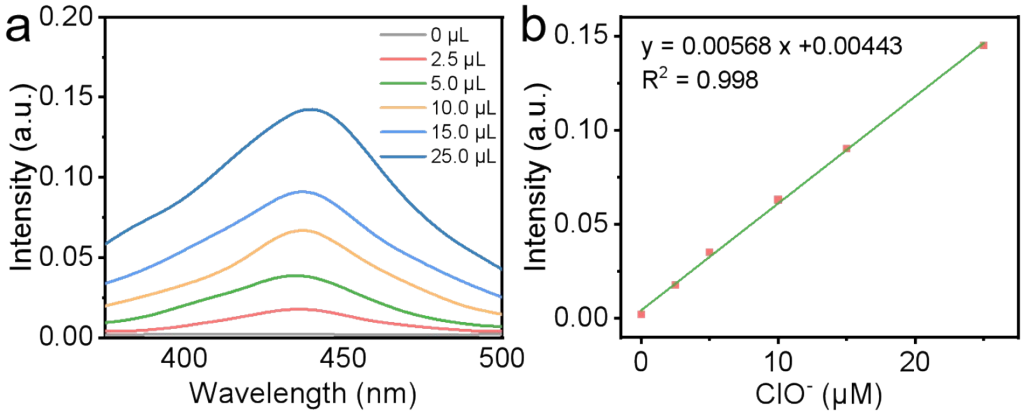

Fig. S12. (a) UV-vis absorption spectra of various active chlorine concentrations. (b) Calibration curve was used to evaluate ClO^- concentrations of the electrolyte.

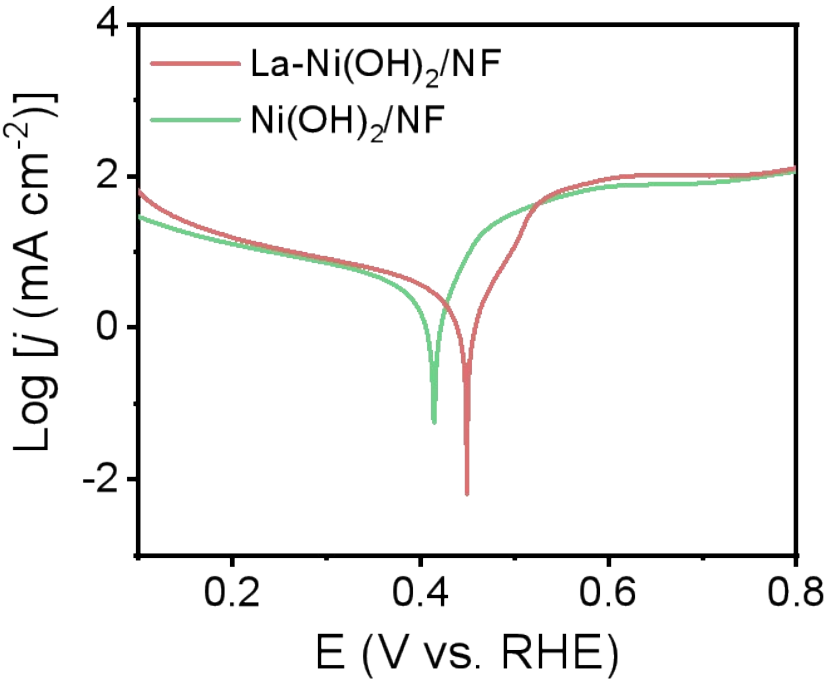

Fig. S13. Corrosion polarization plots of the La-$Ni(OH)_2$/NF and $Ni(OH)_2$/NF electrodes in 1 M KOH + seawater.

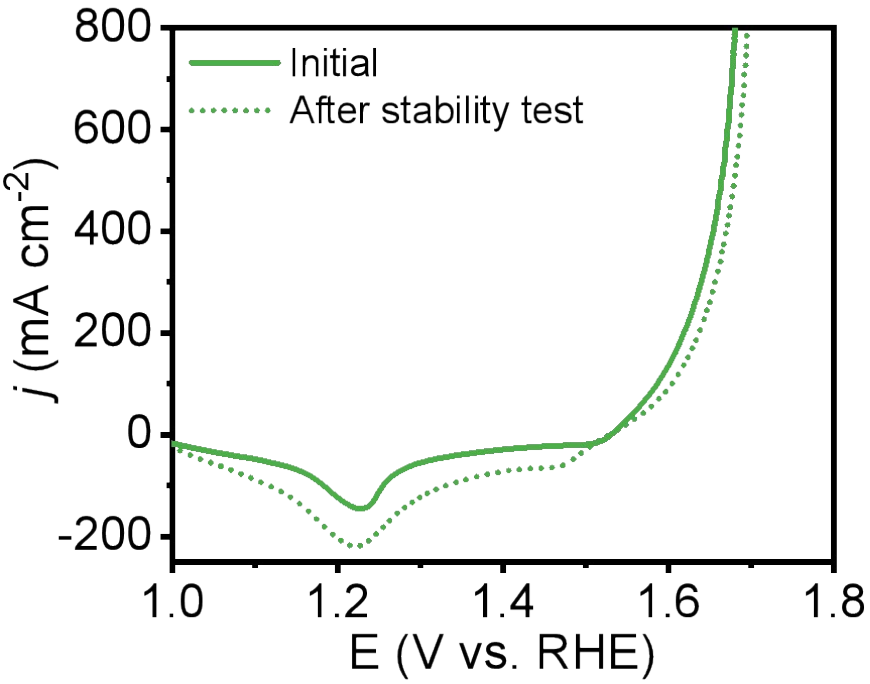

Fig. S14. LSV curves of La-Ni(OH)$_2$/NF before and after the stability test at a current density of 500 mA cm^{-2} in 1 M KOH + seawater.

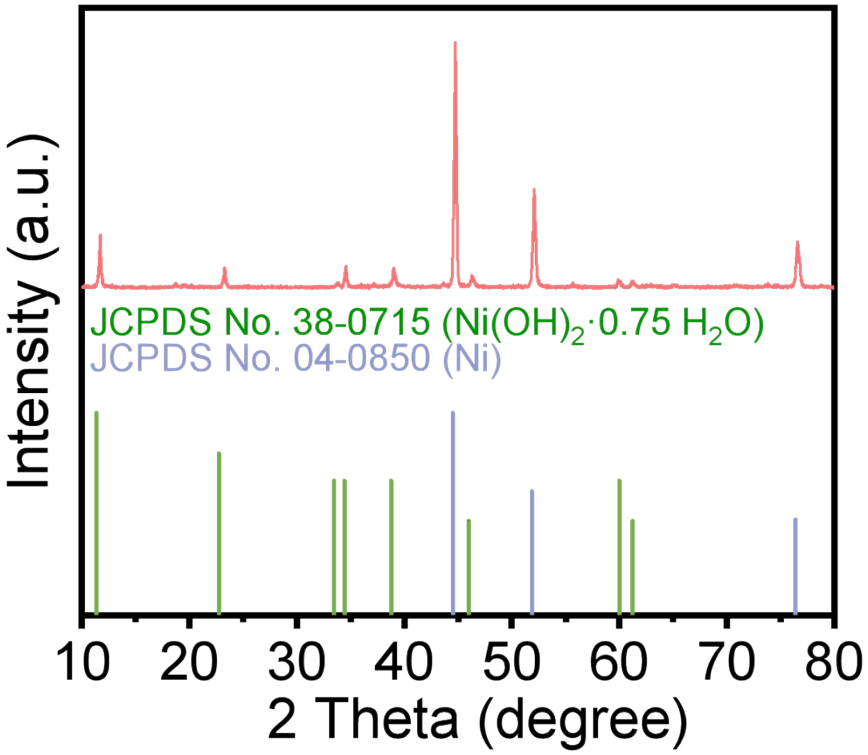

Fig. S15. XRD pattern of La-Ni(OH)$_2$/NF after stability test.

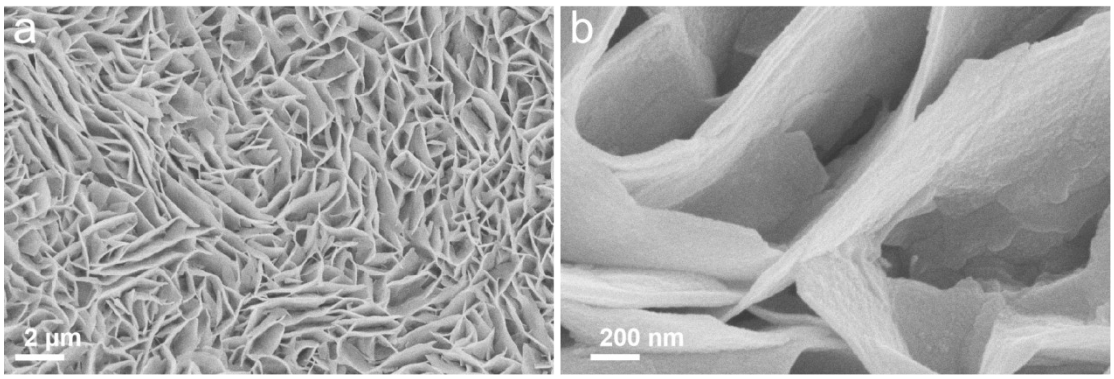

Fig. S16. (a) Low- and (b) high-magnification SEM images of La-$Ni(OH)_2$/NF after stability test in 1 M KOH + seawater.

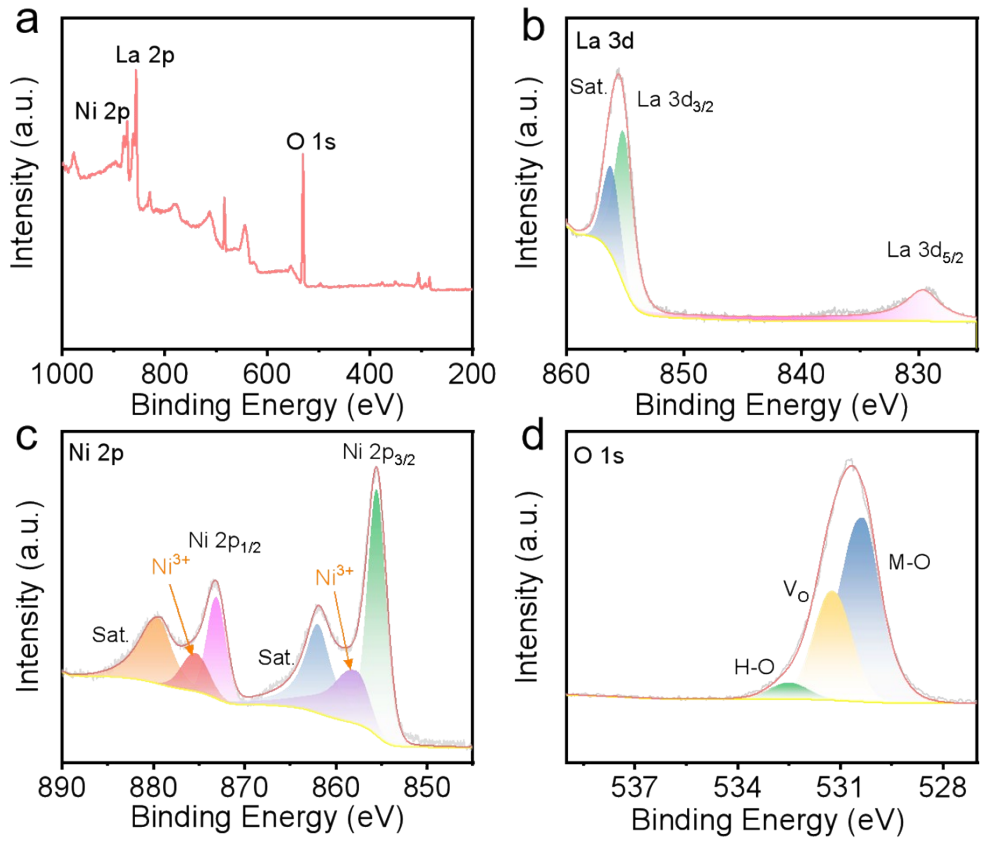

Fig. S17. (a) XPS survey spectrum and high-resolution XPS spectra in the (b) La 3d, (c) Ni 2p, and (d) O 1s regions of La-$Ni(OH)_2$ after stability test.

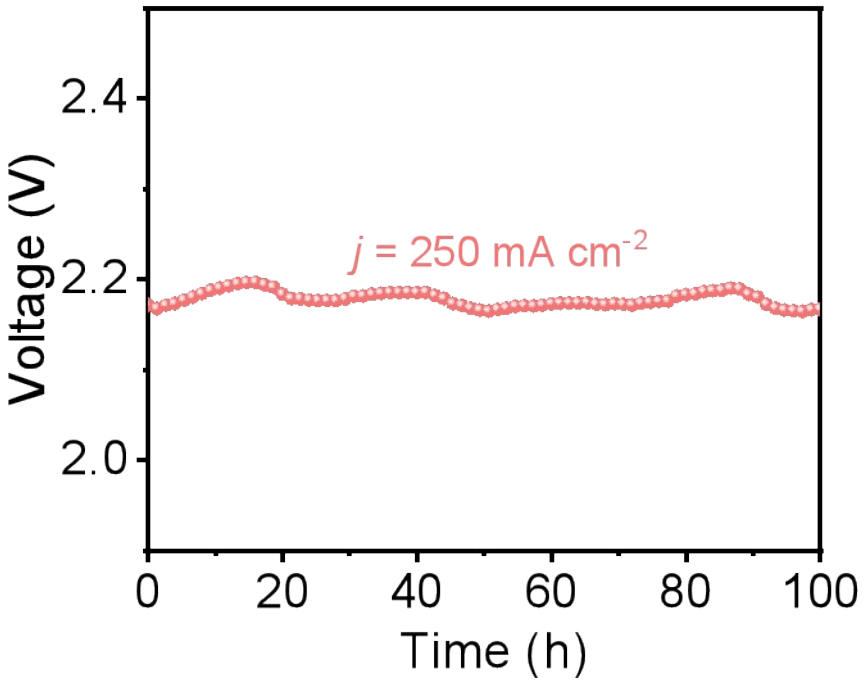

Fig. S18. Long-term operation of Pt/C/NF||La-Ni(OH)$_2$/NF.

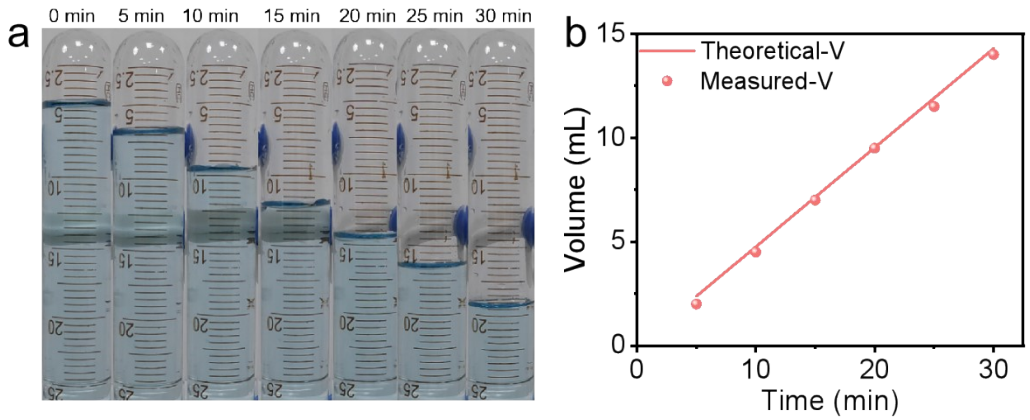

Fig. S19. (a) Digital photographs of the collected H_2 and (b) comparison between the collected and theoretical H_2 amount for Pt/C/NF||La-Ni(OH)$_2$/NF at a j of 250 mA cm^{-2} in alkaline seawater.

Table S1a. Element analysis of La-$Ni(OH)_2$/NF by ICP-OES.

Element	Element concentration (mg/L)	wt. (%)
La	380.667	54.38
Ni	1.225	0.18

Table S1b. Element analysis of La-$Ni(OH)_2$/NF after stability test by ICP-OES.

Element	Element concentration (mg/L)	wt. (%)
La	372.333	53.19
Ni	1.048	0.15

Table S2 Comparison of OER catalytic performance for oxidation of La-$Ni(OH)_2$/NF with reported catalysts.

Catalysts	Current Density (mA cm^{-2})	Overpotential (mV)	Electrolyte	Ref.
La-$Ni(OH)_2$/NF	100	355	1 M KOH + seawater	This work
	500	434	1 M KOH + seawater	
Co-Ni_3S_2/NF	100	368	1 M KOH + seawater	2
$Ni(OH)_2$-TCNQ/GP	100	382	1 M KOH + seawater	3
	500	542	1 M KOH + seawater	
Ni_3S_2-MoS_2-Ni_3S_2/NF	100	410	1 M KOH + seawater	4
Cr-CoCH/NF	100	394	1 M KOH + seawater	5
	500	450	1 M KOH + seawater	
NiCoHPi@Ni_3N/NF	100	396	1 M KOH + seawater	6
	500	474	1 M KOH + seawater	
$CoSe_2$-NCF	100	455	1 M KOH	7
$NiCo_2O_4$/CC	100	360	1 M KOH + seawater	8
Pd-CoNPs@C	100	429	1 M KOH + seawater	9
ZIF67-derived Co-CoO@C	10	374	1 M KOH + seawater	10
$Ni_5Mo/NiCo_2O_4$/NF	50	305	1 M KOH + seawater	11
NiCoS/NF	100	360	1 M KOH + seawater	12
	500	440	1 M KOH + seawater	
NRAHM-NiO/NF	100	356	1 M KOH + seawater	13
	300	684	1 M KOH + seawater	

$NiSe_2$@NiOOH/NF	100	360	1 M KOH + seawater	14
	500	460	1 M KOH + seawater	

References

1 L. Zhang, J. Liang, X. He, Q. Yang, Y. Luo, D. Zheng, S. Sun, J. Zhang, H. Yan, B. Ying, X. Guo and X. Sun, *Inorg. Chem. Front.*, 2023, **10**, 2100–2106.

2 M. Yue, X. He, S. Sun, Y. Sun, M. S. Hamdy, M. Benaissa, A. A. M. Salih, J. Liu and X. Sun, *Nano Res.*, 2024, **17**, 1050–1055.

3 L. Zhang, J. Wang, P. Liu, J. Liang, Y. Luo, G. Cui, B. Tang, Q. Liu, X. Yan, H. Hao, M. Liu, R. Gao and X. Sun, *Nano Res.*, 2022, **15**, 6084–6090.

4 Y. Li, X. Wu, J. Wang, H. Wei, S. Zhang, S. Zhu, Z. Li, S. Wu, H. Jiang and Y. Liang, *Electrochim. Acta*, 2021, **390**, 138833.

5 M. Zhang, X. He, K. Dong, H. Zhang, Y. Yao, C. Yang, M. Yue, S. Sun, Y. Sun, D. Zheng, Y. Luo, Q. Liu, N. Li, B. Tang, J. Liu and X. Sun, *Chem. Commun.*, 2023, **59**, 9750–9753.

6 H. Sun, J. Sun, Y. Song, Y. Zhang, Y. Qiu, M. Sun, X. Tian, C. Li, Z. Lv and L. Zhang, *ACS Appl. Mater. Interfaces*, 2022, **14**, 22061–22070.

7 H. Chen, S. Zhang, Q. Liu, P. Yu, J. Luo, G. Hu and X. Liu, *Inorg. Chem. Commun.*, 2022, **146**, 110170.

8 J. Yang, Y. Wang, J. Yang, Y. Pang, X. Zhu, Y. Lu, Y. Wu, J. Wang, H. Chen, Z. Kou, Z. Shen, Z. Pan and J. Wang, *Small*, 2022, **18**, 2106187.

9 Z. K. Ghouri, D. J. Hughes, K. Ahmed, K. Elsaid, M. M. Nasef, A. Badreldin and A. Abdel-Wahab, *Sci. Rep.*, 2023, **13**, 20866.

10 S. Fathima T.K., A. Ghosh and S. Ramaprabhu, *Int. J. Hydrogen Energy*, 2024, **49**, 780–793.

11 H. Chen, S. Qiao, J. Yang and X. Du, *Mol. Catal.*, 2022, 518, 112086.

12 C. Wang, M. Zhu, Z. Cao, P. Zhu, Y. Cao, X. Xu, C. Xu and Z. Yin, *Appl. Catal. B-Environ*, 2021, **291**, 120071.

13 K. Hemmati, A. Kumar, A. R. Jadhav, O. Moradlou, A. Z. Moshfegh and H. Lee, *ACS Catal.*, 2023, **13**, 5516−5528.

14 H. Zhang, X. He, K. Dong, Y. Yao, S. Sun, M. Zhang, M. Yue, C. Yang, D. Zheng, Q. Liu, Y. Luo, B. Ying, S. Alfaifi, X. Ji, B. Tang and X. Sun, *Mater. Today Phys.*, 2023, **38**, 101249.